Responses of the field-aligned currents in the plasma sheet boundary layer to a geomagnetic storm

YuanQiang Chen[1,2]*, MingYu Wu[1,2]*, YangJun Chen[1], SuDong Xiao[1], GuoQiang Wang[1], and TieLong Zhang[1,3,4]*

[1]Shenzhen Key Laboratory of Numerical Prediction for Space Storm, Harbin Institute of Technology, Shenzhen 518055, China;

[2]Key Laboratory of Solar Activity and Space Weather, National Space Science Center, Chinese Academy of Sciences, Beijing 100190, China;

[3]Chinese Academy of Sciences, Center for Excellence in Comparative Planetology, Hefei 230026, China;

[4]Space Research Institute, Austrian Academy of Sciences, Graz 8042, Austria

Key Points:
- The magnitudes of field-aligned currents are strongest in the main phase, weaker in the recovery phase, and weakest in the quiet period.
- Most of the field-aligned currents are carried by electrons, although ions can also be significant during a storm time.

Abstract: Geomagnetic storms can result in large magnetic field disturbances and intense currents in the magnetosphere and even on the ground. As an important medium of momentum and energy transport among the solar wind, magnetosphere, and ionosphere, field-aligned currents (FACs) can also be strengthened in storm times. This study shows the responses of FACs in the plasma sheet boundary layer (PSBL) observed by the Magnetospheric Multiscale (MMS) spacecraft in different phases of a large storm that lasted from May 27, 2017, to May 29, 2017. Most of the FACs were carried by electrons, and several FACs in the storm time also contained sufficient ion FACs. The FAC magnitudes were larger in the storm than in the quiet period, and those in the main phase were the strongest. In this case, the direction of the FACs in the main phase showed no preference for tailward or earthward, whereas the direction of the FACs in the recovery phase was mostly tailward. The results suggest that the FACs in the PSBL are closely related to the storm and could be driven by activities in the tail region, where the energy transported from the solar wind to the magnetosphere is stored and released as the storm is evolving. Thus, the FACs are an important medium of energy transport between the tail and the ionosphere, and the PSBL is a significant magnetosphere–ionosphere coupling region in the nightside.

Keywords: field-aligned currents; plasma sheet boundary layer; geomagnetic storm

1. Introduction

Considerable momentum and energy can penetrate into the magnetosphere and ionosphere from the solar wind during geomagnetic storms, which can then result in large magnetic field disturbances and geomagnetic-induced currents on the ground (Gonzalez et al., 1994; Milan et al., 2017; Zong QG and Zhang H, 2018; Ma X et al., 2020; Otsuka et al., 2021; Wang YB et al., 2023). One important medium for the momentum and energy transport among the solar wind, magnetosphere, and ionosphere is field-aligned currents (FACs), which can become very intense during storms, substorms, or both (Milan et al., 2017; McPherron et al., 2018; Cowley, 2000; Balachandran et al., 2021). At an ionospheric altitude, large-scale FAC systems have been termed Region 1 and

Region 2 current systems, which are generally around the auroral region (Iijima and Potemra, 1978). Region 1 currents flow into the ionosphere on the dawnside and out of the ionosphere on the duskside, whereas Region 2 currents flow in the opposite direction. Magnetic reconnection at the subsolar magnetopause in the dayside can drive Region 1 currents (Anderson et al., 2016), and Region 2 currents may connect to ring currents (Le et al., 2004; Ganushkina et al., 2018; Imajo et al., 2018). The plasma sheet boundary layer (PSBL) is an important magnetosphere–ionosphere coupling region in the nightside. It lies between the plasma sheet and the lobe and is characterized by field-aligned distributed particles. Dominant magnetic field components align the *X*–*Y* plane in the geocentric solar magnetospheric (GSM) coordinate system (Eastman et al., 1984; Baumjohann et al., 1989). The Region 1 and Region 2 currents could connect to the tail region via the FACs in the PSBL (Elphic et al., 1985; Ohtani et al., 1988; Shi JK et al., 2010). These FACs could be a part of the substorm current wedge and associate with various processes in the tail region, such as the bursty bulk flow and dipolarization fronts in the plasma sheet (Angelopoulos et al., 1994; Kepko et al., 2015; Nakamura et al.,

2017; Schmid et al., 2019; Wang GQ et al., 2021).

Recently, Chen YQ et al. (2019, 2021) analyzed the properties of FACs in the PSBL by using Magnetospheric Multiscale (MMS) mission observations. They found that the occurrence rate of FACs increased when the magnetosphere became active and that the FAC magnitudes intensified. Most of the FACs were carried by thermal electrons, although during the active period, the contribution to FACs from cold electrons would increase. Cheng ZW et al. (2016) used Cluster observations to demonstrate that ions could also contribute to FACs in the PSBL during a substorm. Their studies suggest that FACs in the PSBL are closely related to the level of magnetosphere activity (Ohtani et al., 1988; Shi JK et al., 2010; Nakamura et al., 2017; McPherron et al., 2018; Chen YQ et al., 2021).

Nevertheless, how the FACs in the PSBL respond to a storm has scarcely been demonstrated (Ohtani et al., 1988), although statistical analyses have indicated stronger FACs during the active period (Chen YQ et al., 2021). Owing to the high accuracy and high sampling rate of magnetic field data and plasma measurements from the four MMS spacecraft (Burch et al., 2016), we were able to obtain more reliable FAC densities and their carriers than in the observations made by earlier spacecraft (Phan et al., 2016; Chen YQ et al., 2019, 2021). In this study, we present the MMS observations in the PSBL in different phases of a geomagnetic storm to demonstrate the responses of the FACs to the storm and to illustrate that the FACs in the PSBL are important media of magnetosphere–ionosphere energy coupling in the nightside.

2. Observations

Four identical MMS spacecraft were launched on March 12, 2015, and the distances between them are ~10–400 km (Burch et al., 2016). Their orbital inclination is ~28° and their orbital apogee is ~12 or ~25 R_E (Earth radius) depending on their scientific phase. The fluxgate magnetometer (Russell et al., 2016) is able to provide

magnetic field vectors up to 128 Hz. The Fast Plasma Investigation (FPI; Pollock et al., 2016) can provide plasma measurements at a high sampling rate (30 ms for electrons and 150 ms for ions). In this study, magnetic field data at 16 Hz and plasma moments at 4.5 s were used. The geomagnetic storm or substorm was indicated by the magnetic indices from SuperMAG (https://supermag.jhuapl.edu).

The top panel of Figure 1 shows the SuperMag symmetric ring current (SMR) index, which illustrates that a large geomagnetic storm began at approximately 15:00 on May 27, 2017, and lasted for several days. The SMR index was derived from the magnetometer data provided by the SuperMAG collaborators and is analogous to the *Dst* (disturbance storm time) index (Gjerloev, 2012; Newell and Gjerloev, 2012). The main phase of the storm lasted from ~21:00 on May 27, 2017, to ~07:00 on May 28, 2017, and during this time interval, a severe substorm occurred, as indicated by the auroral electrojet indices (i.e., SuperMag auroral electrojet upper envelopes (SMU) [black] and SuperMag auroral electrojet lower envelopes (SML) [red] shown in the bottom panel of Figure 1). The SMU and SML were also obtained from SuperMAG and are analogous to the auroral electrojet upper envelopes (AU) and auroral electrojet lower envelopes (AL) indices, respectively (Newell and Gjerloev, 2011). The SMR reached almost −150 nT, and the SML reached almost −1800 nT. After ~07:00 on May 28, 2017, the storm evolved into its recovery phase and lasted until ~09:00 on May 29, 2017. Two relatively smaller substorms then occurred at ~13:00 on May 29, 2017, and at ~04:00 on May 30, 2017. After 12:00 on May 30, 2017, the magnetosphere was returned to the quiet period.

Considering the availability of the MMS observations in the tail region, we chose four time intervals:

(I) From 22:25 on May 27, 2017, to 00:05 on May 28, 2017, which was in the main phase of the storm and is marked by the red shaded region in Figure 1. The spacecraft in this time interval were
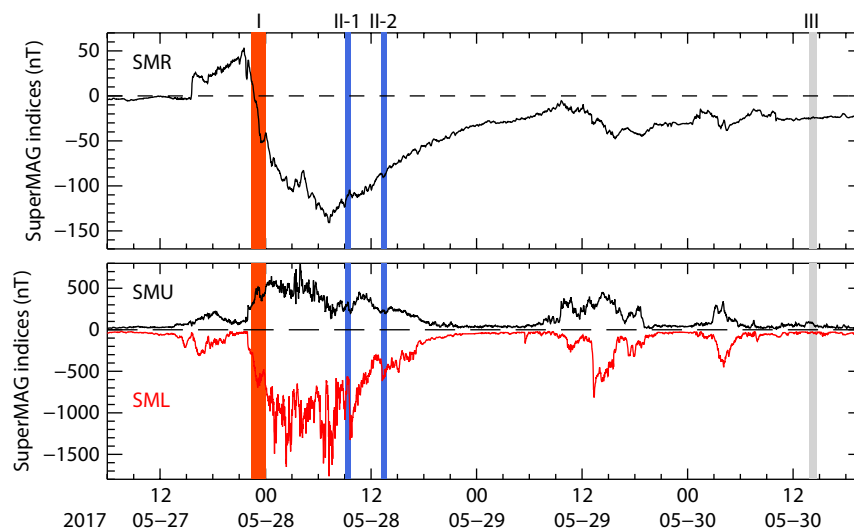
Figure 1. Geomagnetic storm and substorms indicated by SuperMAG indices: (top) SuperMag symmetric ring current (SMR); (bottom) SuperMag auroral electrojet upper envelopes (SMU, black) and SuperMag auroral electrojet lower envelopes (SML, red). The red shaded region indicates the time interval (I) in the main phase, the blue shaded regions indicate the time intervals (II-1, II-2) in the recovery phase, and the gray shaded region indicates the time interval (III) in the quiet period.

around [−18.0, −9.4, −0.8] R_E in GSM.

(II-1, II-2) From 09:00 to 09:40 and from 13:05 to 13:45 on May 28, 2017, which were in the recovery phase of the storm and are marked by the blue shaded regions in Figure 1. The spacecraft in these time intervals were around [−19.9, −14.0, 4.0] R_E in GSM.

(III) From 13:50 to 14:40 on May 30, 2017, which was in the quiet period and is marked by the gray shaded region in Figure 1. The spacecraft in this time interval were around [−16.3, −6.0, 1.4] R_E in GSM.

Figure 2 then shows the MMS1 observations of the magnetic field and plasma during these four time intervals. Figure 2-Ia shows the magnitude (B_t) and three components (B_x, B_y, B_z) of the magnetic field in GSM coordinates; Figure 2-Ib shows the ion omnidirectional energy flux; Figure 2-Ic shows the electron omnidirectional energy flux; Figure 2-Id shows the plasma β, which is the ratio of the plasma thermal pressure to the magnetic pressure; and Figure 2-Ie shows the magnitude of the FACs, in which J_B (cyan line) represents the FACs obtained by the curlometer method and the magnetic field data from the four spacecraft, and J_P (black line) represents the FACs obtained by the plasma number density and bulk velocity (Dunlop et al., 2002; Chen YQ et al., 2019, 2021). The other time intervals (II-1, II-2, and III) are shown in the same format.
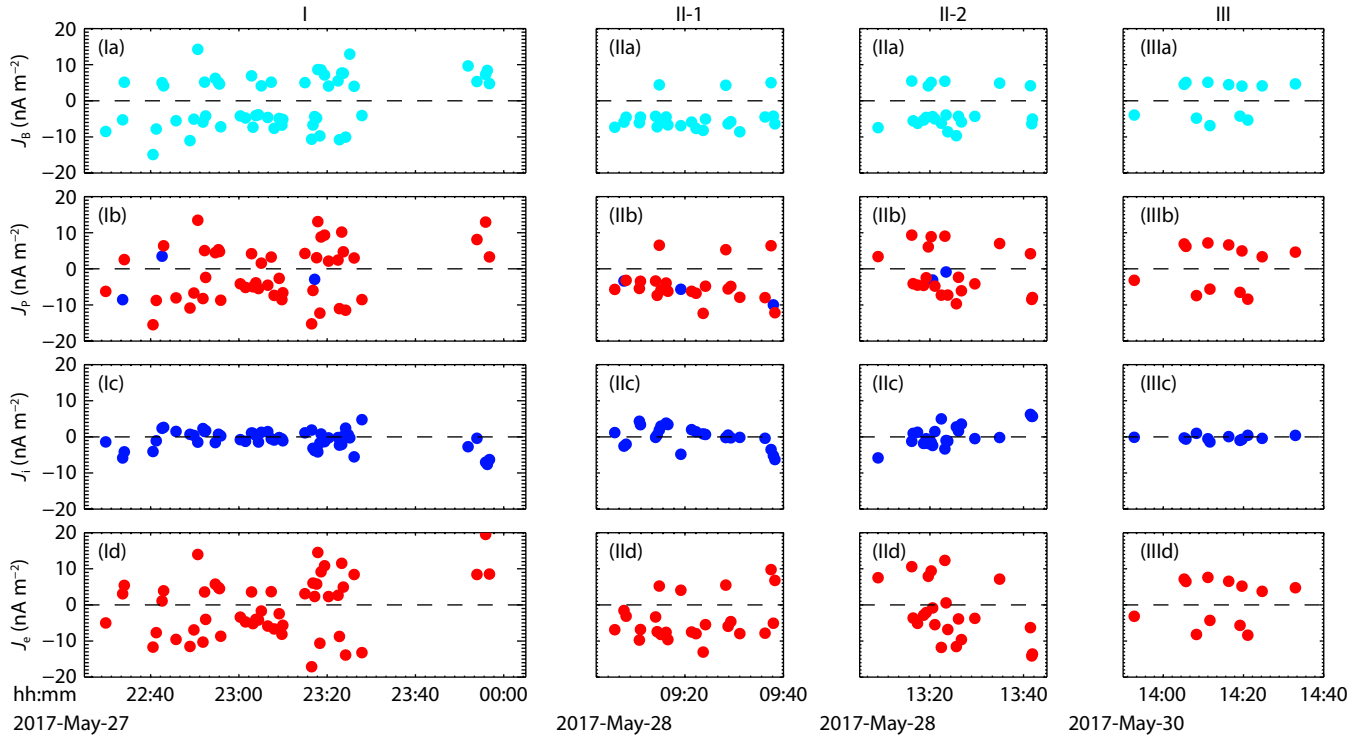
During the four time intervals, the plasma β were mainly in the range of 0.01 to 1.0 and the magnetic field was dominant by the B_x component, suggesting that the MMS spacecraft were in the PSBL (Cheng ZW et al., 2016; Chen YQ et al., 2019, 2021). Overall,

the profiles of J_B and J_P matched each other well. The FACs in those time intervals were analyzed by Chen YQ et al. (2021). They assumed the FAC events were reliable by requiring the results of J_B and J_P to be similar to each other. Details can be found in Chen YQ et al. (2019, 2021). Therefore, we can speculate on the main FAC carriers for those FAC events because their plasma measurements are reliable. The spectra of the ion and electron energy fluxes also suggest that the FPI measurements covered most of the energy channels of the particles well. Here, we have adopted the FAC events found by Chen YQ et al. (2021) in these four time intervals, and the times of those FAC events are marked by the vertical red lines in Figure 2. We observed 55 FACs in time interval I, 46 FACs in time intervals II-1 and II-2, and 12 FACs in time interval III.

The high sampling rate and high accuracy of plasma measurements obtained by the MMS enabled us to recognize the species of the FAC carriers (Phan et al., 2016; Chen YQ et al., 2019). Chen YQ et al. (2021) concluded that ~90% of FACs in the PSBL are mainly contributed by electrons. Most of the electrons are thermal electrons, although the contribution to FACs from cold electrons will increase when the magnetosphere becomes active. The authors illustrated that the occurrence rate of FACs is also larger during the active period than the quiet period. Figure 3 shows scatter plots of the magnitude of the observed FAC events marked in Figure 2. In the following discussion, we consider the ambient magnetic field direction of each FAC event. Accordingly, FACs with a negative magnitude mean the FACs propagate tailward, whereas FACs with a positive magnitude mean the FACs
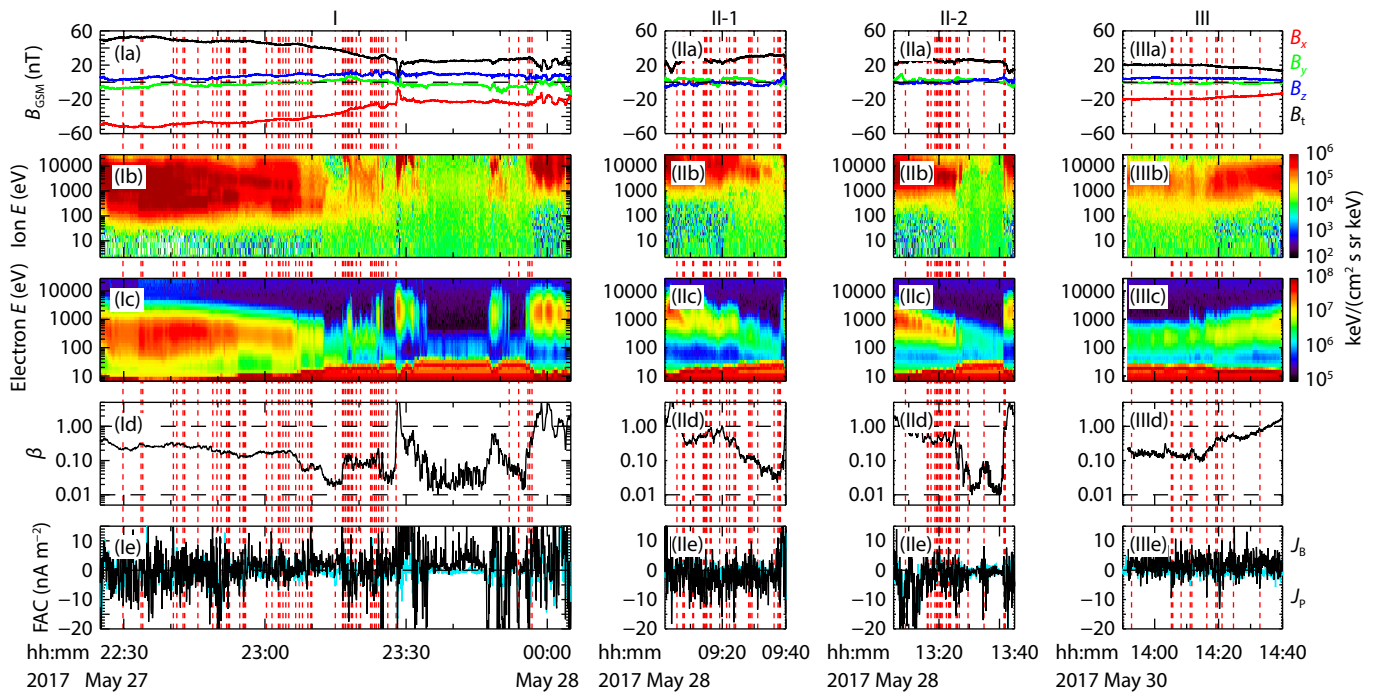
Figure 2. Magnetospheric multiscale observations of the magnetic field and plasma during the four time intervals (I, II-1, II-2, and III). All the time intervals are shown separately in the same format: (a) magnetic field magnitude and components in geocentric solar magnetospheric (GSM) coordinates; (b) ion omnidirectional energy flux (ion E); (c) electron omnidirectional energy flux (electron E); (d) plasma β; (e) field-aligned currents (FACs) obtained by the curlometer method (J_B, cyan line) and plasma moments (J_P, black line). The vertical red lines mark the times of the FAC events analyzed in this study.

Figure 3. Magnitude of the field-aligned current (FAC) events during the four time intervals (I, II-1, II-2, and III). All the time intervals are shown separately in the same format: (a) J_B, FAC magnitude obtained by the curlometer method; (b) J_P, FAC magnitude obtained from the ion FACs and electron FACs, with red circles indicating that the electron FAC is larger than the ion FAC and blue circles representing that the ion FAC is larger; (c) J_i, ion FAC magnitude obtained from the ion number density and bulk velocity; (d) J_e, electron FAC magnitude obtained from the electron number density and bulk velocity. A negative value means the FAC is tailward, and a positive value means the FAC is earthward.

propagate earthward. Figure 3-Ia shows the FAC magnitude of J_B, and Figure 3-Ib shows the FAC magnitude of J_P. The symbol is plotted in red if the electron FAC is larger than the ion FAC, and it is plotted in blue if not. Figures 3-Ic and 3-Id show the ion FACs (blue) and electron FACs (red), respectively. The other time intervals are shown in the same format. As illustrated by panels Ib, IIb, and IIIb, the FACs in the PSBL were mainly carried by electrons. During time interval I, 5 (~9.1%) ion FACs had a magnitude larger than 5 nA·m^{-2}, and 3 ion FACs were stronger than the electron FACs. During the time interval in panels II-1 and II-2, 6 (~13.0%) ion FACs had a magnitude larger than 5 nA·m^{-2}, and 5 ion FACs were stronger than the electron FACs. However, in the quiet period (III), all the FACs were electron FACs, and none of the ion FACs was larger than 5 nA·m^{-2}. The occurrence rate of FACs was also smaller in the quiet period than in the storm time, indicating a strong, dynamic PSBL during the storm.

These FACs were observed in the different phases of the storm. Figure 4 shows the distribution of their magnitudes. The occurrence represents the normalized counts in each bin, and a larger occurrence means more FACs were observed in that bin. The left panel shows the distribution of the absolute value of J_B, and the right panel shows the distribution of J_B. The red histograms represent the FACs observed in the main phase of the storm (I), the blue histograms represent the FACs observed in the recovery phase (II-1, II-2), and the gray histograms represent the FACs observed in the quiet period (III). As shown by the left panel, the magnitudes of the FACs observed during the storm were mainly

in the bin of ~5–10 nA·m^{-2}, whereas those of the FACs observed in the quiet time were mainly in the bin of ~0–5 nA·m^{-2}, suggesting that the FACs in the PSBL were strengthened when the magnetosphere was active. Likewise, the FACs in the main phase were the strongest because some of their magnitudes exceeded 10 nA·m^{-2}, and the FACs in the recovery phase were relatively weaker. The right panel shows that the FAC densities in the main phase generally had an even distribution from −10 to 10 nA·m^{-2} but that the FAC densities in the recovery phase were mostly in the bin of ~−10 to −5 nA·m^{-2}. The negative FACs were tailward, whereas the positive FACs were earthward. Thus, in this case, the FACs in the recovery phase (time intervals II-1 and II-2) were mostly tailward, suggesting the electrons as the FAC carriers were generally moving toward the Earth.

3. Discussion
In this study, we presented the responses of the FACs observed by MMS in the PSBL to a large geomagnetic storm. The FACs observed in the main phase of the storm, the recovery phase of the storm, and the quiet period showed different properties. The magnitudes of the FACs in the main phase were the strongest, and those in the recovery phase were relatively weaker. However, the FAC magnitudes were larger in the storm time than in the quiet period, which is consistent with the statistical results (Chen YQ et al., 2021), as is the occurrence rate of the FACs. The stronger FACs could be the result of a compressed magnetosphere resulting from the large dynamic pressure of the incoming solar wind, which might have caused the large storm, or the energy released
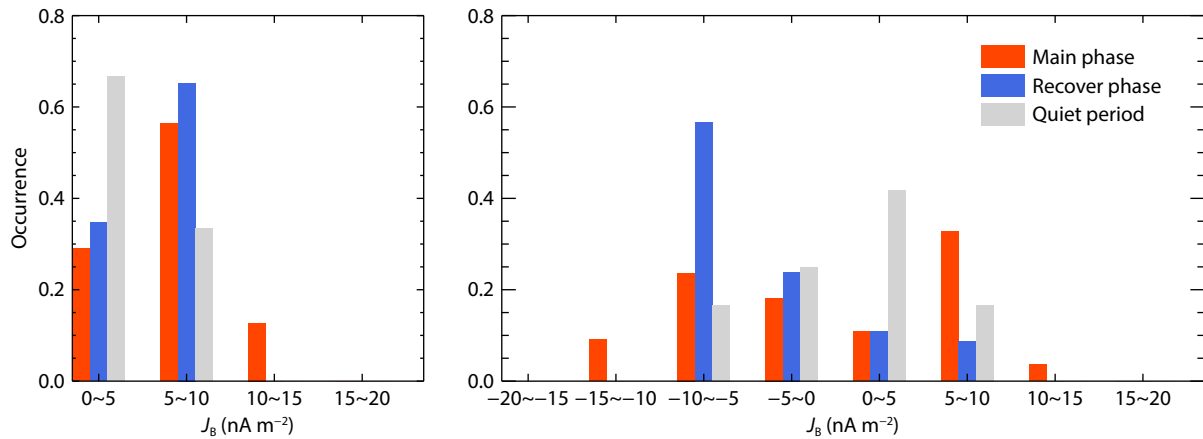
Figure 4. Distribution of the magnitude of the field-aligned currents (FACs) in the main phase (red histograms), the recovery phase (blue histograms), and the quiet period (gray histograms). The counts in each bin have been normalized. The left panel shows the distribution of the absolute value of J_B, and the right panel shows the distribution of J_B. A negative value means the FAC is tailward, and a positive value means the FAC is earthward.

by activities in the tail region, such as magnetic reconnection, as the storm was evolving (Lu S et al., 2018; Nakamura et al., 2018; Wang GQ et al., 2021).

Most of the FACs were carried by electrons, meaning the electron dynamics were more significant in the PSBL. These electrons could be accelerated locally by parallel electric fields during the tail current sheet thinning, or they could be accelerated by magnetic reconnection occurring elsewhere and then move along the magnetic field line to the PSBL (Wang RS et al., 2014; Lu S et al., 2017). Moreover, we were able to observe several FAC events in which the ion FACs were significant. All these ion FACs were observed in the main phase or the recovery phase of the storm. This result suggests a more dynamic PSBL during the active period and that the ions could be transported via the PSBL between the ionosphere and the tail region (Cheng ZW et al., 2016; Nakamura et al., 2017, 2018; Shi JK et al., 2019). However, during the quiet period, the FACs were all carried by electrons. The driver of those electrons could be the potential drop caused by the solar wind motional electric field or local processes, although we could not yet determine the driver here (Ueno et al., 2002; Keiling et al., 2005; Liang J et al., 2016; Wang GQ et al., 2021).

All the FACs were observed on the dawnside by MMS. In this case, the FAC densities in the main phase generally showed an even distribution of negative and positive values, which suggests that these FACs had no preference for flowing earthward or tailward, although the FACs could indicate a rapid momentum and energy exchange between the tail region and ionosphere. The strengthened FACs could be the result of the thinning process of the tail or burst energy release in the tail in the main phase, or both (Dungey, 1961; Gonzalez et al., 1994; Lu S et al., 2017). In the recovery phase, the FAC densities were also intense, whereas they were mostly tailward; thus, the electrons that carried these FACs were flowing earthward. These high-speed earthward electrons were possibly driven by the tail magnetic reconnection (Lu QM et al., 2010; Wang RS et al., 2014), which could transport sufficient energy into the inner magnetosphere or ionosphere. The direction of the FACs in the recovery phase showed the Region 2 current sense,

namely, flow out of the ionosphere (tailward) in the dawnside (Elphic et al., 1985). Therefore, these FACs could also represent the current circuit that connects the ionospheric currents to the current system in the tail region, probably the substorm current wedge (Kepko et al., 2015; Nakamura et al., 2017).

4. Conclusions

This work shows the FACs in the PSBL observed by the MMS spacecraft in different phases of a large geomagnetic storm. The FACs were mostly carried by electrons, except for several FACs in the storm time that had significant contributions from ions. The FAC magnitudes in the main phase were the strongest and could exceed 10 nA·m^{-2}. The FAC magnitudes in the recovery phase were slightly weaker and mostly in the range of ~5–10 nA·m^{-2}. And the FAC magnitudes in the quiet period were the weakest and were mostly smaller than 5 nA·m^{-2}. These results indicate that the FACs were strengthened in the storm time, especially in the main phase, possibly because of the energy transported from the solar wind into the magnetosphere. All the FACs were observed on the dawnside. In this case, we found that the FAC densities in the main phase showed no preference for tailward or earthward, whereas the FAC densities in the recovery phase mostly flowed tailward. This result suggests that the FACs in different phases of the storm could be driven by different activities in the tail region. The results shown in this work indicate FACs in the PSBL are an important medium of energy transport between the tail and the inner magnetosphere or ionosphere during a storm.

References

Anderson, B. J., Russell, C. T., Strangeway, R. J., Plaschke, F., Magnes, W., Fischer, D., Korth, H., Merkin, V. G., Barnes, R. J., ... Cohen, I. J. (2016). Electrodynamic context of magnetopause dynamics observed by Magnetospheric Multiscale. *Geophys. Res. Lett.*, *43*(12), 5988–5996. https://doi.org/10.1002/2016GL069577

Angelopoulos, V., Kennel, C. F., Coroniti, F. V., Pellat, R., Kivelson, M. G., Walker, R. J., Russell, C. T., Baumjohann, W., Feldman, W. C., and Gosling, J. T. (1994). Statistical characteristics of bursty bulk flow events. *J. Geophys. Res.: Space Phys.*, *99*(A11), 21257–21280. https://doi.org/10.1029/94JA01263

Balachandran, R., Chen, L.-J., Wang, S., and Fok, M.-C. (2021). Correlating the interplanetary factors to distinguish extreme and major geomagnetic storms. *Earth Planet. Phys.*, *5*(2), 180–186. https://doi.org/10.26464/epp2021015

Baumjohann, W., Paschmann, G., and Cattell, C. A. (1989). Average plasma properties in the central plasma sheet. *J. Geophys. Res.*, *94*(A6), 6597–6606. https://doi.org/10.1029/JA094iA06p06597

Burch, J. L., Moore, T. E., Torbert, R. B., and Giles, B. L. (2016). Magnetospheric Multiscale overview and science objectives. *Space Sci. Rev.*, *199*(1–4), 5–21. https://doi.org/10.1007/s11214-015-0164-9

Chen, Y. Q., Wu, M. Y., Wang, G. Q., Schmid, D., Zhang, T. L., Nakamura, R., Baumjohann, W., Burch, J. L., Giles, B. J., and Russell, C. T. (2019). Carriers of the field-aligned currents in the plasma sheet boundary layer: An MMS multicase study. *J. Geophys. Res.: Space Phys.*, *124*(4), 2873–2886. https://doi.org/10.1029/2018JA026216

Chen, Y. Q., Wu, M., Zhang, T. L., Huang, Y., Wang, G. Q., Nakamura, R., Baumjohann, W., Russell, C. T., Giles, B. J., and Burch, J. L. (2021). Statistical characteristics of field-aligned currents in the plasma sheet boundary layer. *J. Geophys. Res.: Space Phys.*, *126*(2), e2020JA028319. https://doi.org/10.1029/2020JA028319

Cheng, Z. W., Zhang, J. C., Shi, J. K., Kistler, L. M., Dunlop, M., Dandouras, I., and Fazakerley, A. (2016). The particle carriers of field-aligned currents in the Earth's magnetotail during a substorm. *J. Geophys. Res.: Space Phys.*, *121*(4), 3058–3068. https://doi.org/10.1002/2015JA022071

Cowley, S. W. H. (2000). Magnetosphere-ionosphere interactions: A tutorial review. In S. I. Ohtani et al. (Eds.), *Magnetospheric Current Systems*. Washington: American Geophysical Union. https://doi.org/10.1029/GM118p0091

Dungey, J. W. (1961). Interplanetary magnetic field and the auroral zones. *Phys. Rev. Lett.*, *6*(2), 47–48. https://doi.org/10.1103/PhysRevLett.6.47

Dunlop, M. W., Balogh, A., Glassmeier, K. H., and Robert, P. (2002). Four-point cluster application of magnetic field analysis tools: The curlometer. *J. Geophys. Res.: Space Phys.*, *107*(A11), 1384. https://doi.org/10.1029/2001JA005088

Eastman, T. E., Frank, L. A., Peterson, W. K., and Lennartsson, W. (1984). The plasma sheet boundary layer. *J. Geophys. Res.: Space Phys.*, *89*(A3), 1553–1572. https://doi.org/10.1029/JA089iA03p01553

Elphic, R. C., Mutch, P. A., and Russell, C. T. (1985). Observations of field-aligned currents at the plasma sheet boundary: An ISEE-1 and 2 survey. *Geophys. Res. Lett.*, *12*(10), 631–634. https://doi.org/10.1029/GL012i010p00631

Ganushkina, N. Y., Liemohn, M. W., and Dubyagin, S. (2018). Current systems in the Earth's magnetosphere. *Rev. Geophys.*, *56*(2), 309–332. https://doi.org/10.1002/2017RG000590

Gjerloev, J. W. (2012). The SuperMAG data processing technique. *J. Geophys. Res.: Space Phys.*, *117*(A9), A09213. https://doi.org/10.1029/2012JA017683

Gonzalez, W. D., Joselyn, J. A., Kamide, Y., Kroehl, H. W., Rostoker, G., Tsurutani, B. T., and Vasyliunas, V. M. (1994). What is a geomagnetic storm? *J. Geophys. Res.: Space Phys.*, *99*(A4), 5771–5792. https://doi.org/10.1029/93JA02867

Iijima, T., and Potemra, T. A. (1978). Large-scale characteristics of field-aligned currents associated with substorms. *J. Geophys. Res.: Space Phys.*, *83*(A2), 599–615. https://doi.org/10.1029/JA083iA02p00599

Imajo, S., Nosé, M., Matsuoka, A., Kasahara, S., Yokota, S., Teramoto, M., Keika, K., Motoba, T., Anderson, B., ... Miyoshi, Y. (2018). Magnetosphere-ionosphere connection of storm-time region-2 field-aligned current and ring current: Arase and AMPERE observations. *J. Geophys. Res.: Space Phys.*, *123*(11), 9545–9559. https://doi.org/10.1029/2018JA025865

Keiling, A., Parks, G. K., Wygant, J. R., Dombeck, J., Mozer, F. S., Russell, C. T., Streltsov, A. V., and Lotko, W. (2005). Some properties of Alfvén waves: Observations in the tail lobes and the plasma sheet boundary layer. *J. Geophys. Res.: Space Phys.*, *110*(A10), A10S11. https://doi.org/10.1029/2004JA010907

Kepko, L., McPherron, R. L., Amm, O., Apatenkov, S., Baumjohann, W., Birn, J., Lester, M., Nakamura, R., Pulkkinen, T. I., and Sergeev, V. (2015). Substorm current wedge revisited. *Space Sci. Rev.*, *190*(1), 1–46. https://doi.org/10.1007/s11214-014-0124-9

Le, G., Russell, C. T., and Takahashi, K. (2004). Morphology of the ring current derived from magnetic field observations. *Ann. Geophys.*, *22*(4), 1267–1295. https://doi.org/10.5194/angeo-22-1267-2004

Liang, J., Lin, Y., Johnson, J. R., Wang, X. Y., and Wang, Z. X. (2016). Kinetic Alfvén waves in three-dimensional magnetic reconnection. *J. Geophys. Res.: Space Phys.*, *121*(7), 6526–6548. https://doi.org/10.1002/2016JA022505

Lu, Q. M., Huang, C., Xie, J. L., Wang, R. S., Wu, M. Y., Vaivads, A., and Wang, S. (2010). Features of separatrix regions in magnetic reconnection: Comparison of 2-D particle-in-cell simulations and Cluster observations. *J. Geophys. Res.*, *115*(A11), A11208. https://doi.org/10.1029/2010JA015713

Lu, S., Artemyev, A. V., and Angelopoulos, V. (2017). Electron cooling and isotropization during magnetotail current sheet thinning: Implications for parallel electric fields. *J. Geophys. Res.: Space Phys.*, *122*(11), 11389–11401. https://doi.org/10.1002/2017JA024712

Lu, S., Pritchett, P. L., Angelopoulos, V., and Artemyev, A. V. (2018). Formation of dawn-dusk asymmetry in Earth's magnetotail thin current sheet: A three-dimensional particle-in-cell simulation. *J. Geophys. Res.: Space Phys.*, *123*(4), 2801–2814. https://doi.org/10.1002/2017JA025095

Ma, X., Xiang, Z., Ni, B. B., Fu, S., Cao, X., Hua, M., Guo, D. Y., Guo, Y. J., Gu, X. D., Liu, Z. Y., and Zhu, Q. (2020). On the loss mechanisms of radiation belt electron dropouts during the 12 September 2014 geomagnetic storm. *Earth Planet. Phys.*, *4*(6), 598–610. https://doi.org/10.26464/epp2020060

McPherron, R. L., Anderson, B. J., and Chu, X. N. (2018). Relation of field-aligned currents measured by the network of Iridium® spacecraft to solar wind and substorms. *Geophys. Res. Lett.*, *45*(5), 2151–2158. https://doi.org/10.1002/2017GL076741

Milan, S. E., Clausen, L. B. N., Coxon, J. C., Carter, J. A., Walach, M. T., Laundal, K., Østgaard, N., Tenfjord, P., Reistad, J., ... Anderson, B. J. (2017). Overview of solar wind–magnetosphere–ionosphere–atmosphere coupling and the generation of magnetospheric currents. *Space Sci. Rev.*, *206*(1–4), 547–573. https://doi.org/10.1007/s11214-017-0333-0

Nakamura, R., Nagai, T., Birn, J., Sergeev, V. A., Le Contel, O., Varsani, A., Baumjohann, W., Nakamura, T., Apatenkov, S., ... Turner, D. L. (2017). Near-Earth plasma sheet boundary dynamics during substorm dipolarization. *Earth Planets Space*, *69*(1), 129. https://doi.org/10.1186/s40623-017-0707-2

Nakamura, R., Varsani, A., Genestreti, K. J., Le Contel, O., Nakamura, T., Baumjohann, W., Nagai, T., Artemyev, A., Birn, J., ... Turner, D. L. (2018). Multiscale currents observed by MMS in the flow braking region. *J. Geophys. Res.: Space Phys.*, *123*(2), 1260–1278. https://doi.org/10.1002/2017JA024686

Newell, P. T., and Gjerloev, J. W. (2011). Evaluation of SuperMAG auroral electrojet indices as indicators of substorms and auroral power. *J. Geophys. Res.*, 116(A12), A12211. https://doi.org/10.1029/2011JA016779

Newell, P. T., and Gjerloev, J. W. (2012). SuperMAG-based partial ring current indices. *J. Geophys. Res.*, 117(A5), A05215. https://doi.org/10.1029/2012JA017586

Ohtani, S., Kokubun, S., Elphic, R. C., and Russell, C. T. (1988). Field-aligned current signatures in the near-tail region: 1. ISEE observations in the plasma sheet boundary layer. *J. Geophys. Res.: Space Phys.*, 93(A9), 9709–9720. https://doi.org/10.1029/JA093iA09p09709

Otsuka, Y., Shinbori, A., Sori, T., Tsugawa, T., Nishioka, M., and Huba, J. D. (2021). Plasma depletions lasting into daytime during the recovery phase of a geomagnetic storm in May 2017: Analysis and simulation of GPS total electron content observations. *Earth Planet. Phys.*, 5(5), 427–434. https://doi.org/10.26464/epp2021046

Phan, T. D., Eastwood, J. P., Cassak, P. A., Øieroset, M., Gosling, J. T., Gershman, D. J., Mozer, F. S., Shay, M. A., Fujimoto, M., ... Wilder, F. D. (2016). MMS observations of electron-scale filamentary currents in the reconnection exhaust and near the X line. *Geophys. Res. Lett.*, 43(12), 6060–6069. https://doi.org/10.1002/2016GL069212

Pollock, C., Moore, T., Jacques, A., Burch, J., Gliese, U., Saito, Y., Omoto, T., Avanov, L., Barrie, A., ... Zeuch, M. (2016). Fast Plasma Investigation for Magnetospheric Multiscale. *Space Sci. Rev.*, 199(1–4), 331–406. https://doi.org/10.1007/s11214-016-0245-4

Russell, C. T., Anderson, B. J., Baumjohann, W., Bromund, K. R., Dearborn, D., Fischer, D., Le, G., Leinweber, H. K., Leneman, D., ... Richter, I. (2016). The magnetospheric multiscale magnetometers. *Space Sci. Rev.*, 199(1–4), 189–256. https://doi.org/10.1007/s11214-014-0057-3

Schmid, D., Volwerk, M., Plaschke, F., Nakamura, R., Baumjohann, W., Wang, G. Q., Wu, M. Y., and Zhang, T. L. (2019). A statistical study on the properties of dips ahead of dipolarization fronts observed by MMS. *J. Geophys. Res.: Space Phys.*, 124(1), 139–150. https://doi.org/10.1029/2018JA026062

Shi, J. K., Cheng, Z. W., Zhang, T. L., Dunlop, M., Liu, Z. X., Torkar, K., Fazakerley, A., Lucek, E., Rème, H., ... Shen, C. (2010). South-north asymmetry of field-aligned currents in the magnetotail observed by Cluster. *J. Geophys. Res.*, 115(A7), A07228. https://doi.org/10.1029/2009JA014446

Shi, J. K., Zhang, Z. Y., Torkar, K., Cheng, Z. W., Escoubet, P., Farzakeley, A., Dunlop, M., and Carr, C. (2019). South-north hemispheric asymmetry of the FAE distribution around the cusp region: Cluster observation. *J. Geophys. Res.: Space Phys.*, 124(7), 5342–5352. https://doi.org/10.1029/2019JA026582

Ueno, G., Ohtani, S., Saito, Y., and Mukai, T. (2002). Field-aligned currents in the outermost plasma sheet boundary layer with Geotail observation. *J. Geophys. Res.: Space Phys.*, 107(A11), 32-1-SMP 32-10. https://doi.org/10.1029/2002JA009367

Wang, G. Q., Zhang, T. L., Wu, M. Y., Xiao, S. D., Wang, G., Chen, Y. Q., Sun, J. C., and Volwerk, M. (2021). Field-aligned currents originating from the chaotic motion of electrons in the tilted current sheet: MMS observations. *Geophys. Res. Lett.*, 48(9), e2020GL088841. https://doi.org/10.1029/2020GL088841

Wang, R. S., Lu, Q. M., Khotyaintsev, Y. V., Volwerk, M., Du, A. M., Nakamura, R., Gonzalez, W. D., Sun, X., Baumjohann, W., ... Wu, M. Y. (2014). Observation of double layer in the separatrix region during magnetic reconnection. *Geophys. Res. Lett.*, 41(14), 4851–4858. https://doi.org/10.1002/2014GL061157

Wang, Y. B., Zhang, Y., Wang, Y. J., Liu, P. F., Cheng, J. X., Li, X. Z., Tang, K., Li, L. G., and Duan, X. W. (2023). Influences of various space current systems on the geomagnetic field in near-Earth space. *Earth Planet. Phys.*, 7(1), 93–99. https://doi.org/10.26464/epp2023010

Zong, Q.-G., and Zhang, H. (2018) In situ detection of the electron diffusion region of collisionless magnetic reconnection at the high-latitude magnetopause. *Earth Planet. Phys.*, 2(3), 231–237. https://doi.org/10.26464/epp2018022